Molecular Beam Scattering of Aligned Oxygen Molecules. The Nature of the Bond in the O_2-O_2 Dimer

Vincenzo Aquilanti,*,† Daniela Ascenzi,† Massimiliano Bartolomei,† David Cappelletti,‡ Simonetta Cavalli,† Miguel de Castro Vìtores,§ and Fernando Pirani†

Contribution from Dipartimento di Chimica and Istituto per le Tecnologie Chimiche, Università di Perugia, I-06123, Perugia, Italy

Received May 24, 1999

Abstract: Molecular beam experiments are reported for collisions between oxygen molecules. Total integral cross sections have been measured as a function of the collision energy with the control of molecular alignment. The low collision energy (in the thermal and subthermal range) and the high angular resolution permit observation of the "glory" effect, manifestation of quantum-mechanical interference, which allows an accurate probe of intermolecular interactions. This first complete experimental characterization of the interaction yields a ground (singlet) state bond energy of 17.0 ± 0.8 meV for the most stable dimer geometry (the two oxygen molecules lying parallel at a distance of 3.56 ± 0.07 Å). Also the splittings among the singlet, the triplet, and the quintet surfaces are obtained, and a full representation of their angular dependence is reported via a novel harmonic expansion functional form for diatom−diatom interactions. These results indicate that most of the bonding in the dimer comes from van der Waals forces, but chemical (spin−spin) contributions in this open-shell/open-shell system are not negligible (∼15% of the van der Waals component of the interaction).

Introduction

The first study in which the existence of a weak chemical bond between two oxygen molecules has been proposed dates back to 1924, when G. N. Lewis[1] studied the magnetic susceptibility of liquid oxygen and concluded that oxygen is a mixture of O_2 and O_4 species, the paramagnetic character being given by O_2, while O_4 "*is chemically saturated and also magnetically saturated in the sense that it is not paramagnetic*." He also gave a value of 5.60 meV for the heat of dissociation of the O_2-O_2 dimer.

Actually, the interaction potential in the dimer depends, not only on the distance and relative orientation between the molecules but also on the orientation of the molecular spin ($S = 1$). This results in three distinct potential-energy surfaces corresponding to the singlet, triplet, and quintet states of the dimer arising from different spin coupling of the monomers in the ground electronic state. Spin coupling leads to many peculiar bulk properties of oxygen molecules, but even in the gas phase the intermolecular interaction could deviate from a typical pure van der Waals nature. Linus Pauling, in an early search for a definition of the concept of a chemical bond, stated:[2]

"*In general we do not consider the weak van der Waals forces between molecules as leading to chemical-bond formation; but in exceptional cases, such as that of the O_4 molecule [...] it may happen that these forces are strong enough to make it convenient to describe the corresponding intermolecular interaction as bond formation.*"

The knowledge of the intermolecular interaction potential in the O_2-O_2 dimer is basic to describing scattering processes responsible for energy transfer in the gas phase, transport phenomena in the atmosphere, and spectroscopic features of O_2 in oxygen bulk and to the understanding of O_2 behavior in the condensed phase. The O_2-O_2 dimer shows several weak absorption regions in the Infrared, the red (around 630 and 580 nm), the blue, and the near ultraviolet. These bands have been extensively studied,[3] as for example the absorption bands of the atmosphere of oxygen under pressure and of the liquid, but their analysis is far from complete. Some of these absorption bands in the visible occur in the same wavelength region as the Chappuis bands of ozone and hence can interfere with measurements of stratospheric ozone.[4] Medium-resolution absorption cross sections and high-resolution absorption spectra, in supersonic slit expansion with a rotationally resolved structure,[5] have recently been observed for both visible bands in the red. The photochemistry of the oxygen dimer has been investigated in the ultraviolet range.[6] The interaction between oxygen molecules affects the magnetic couplings and dynamics in solid O_2,[7] which is considered one of the most interesting molecular crystals because of its peculiar structural and magnetic properties. Solid oxygen can, in fact, exist in three different phases: the α phase which is orientationally and magnetically ordered (antiferromagnetic), the β phase which is also orientationally ordered and

* Corresponding author: (phone) 39 75 585 5512; (fax) 39 75 585 5606; (e-mail) aquila@dyn.unipg.it.

† Dipartimento di Chimica.

‡ Istituto per le Tecnologie Chimiche.

§ Present address: Unidad de Láseres y Haces Moleculares, Universidad Complutense de Madrid, 28040 Madrid, Spain.

(1) Lewis, G. N. *J. Am. Chem. Soc.* **1924**, *46*, 2027−2032.

(2) Pauling, L. *The nature of the chemical bond*, 3rd ed.; Cornell University Press: Ithaca, N.Y., 1960; p 6.

(3) Orlando, J. J.; Tyndall, G. S.; Nickerson, K. E.; Calvert, J. G. *Geophys. Res. Lett.* **1991**, *96*, 20755−20760, and references therein.

(4) Perner, D.; Platt, U. *Geophys. Res. Lett.* **1980**, *7*, 1053−1056.

(5) Bussery, B.; Bacis, R.; Biennier, L.; Campargue, A.; Churassy, S.; Jost, R.; Kachanov, A.; Veyret, V. *Chem. Phys. Lett.* **1998**, *288*, 734−742.

(6) Brown, L.; Vaida, V. *J. Phys. Chem.* **1996**, *100*, 7849−7853.

(7) DeFotis, G. C. *Phys. Rev. B* **1981**, *23*, 4714−4739; Meier, R. J.; Shinkel, C. J.; de Visser, A. *J. Phys. C: Solid State Phys.* **1982**, *15*, 1015−1024; Meier, R. J. *Phys. Lett. A* **1983**, *95A*, 115−117; Etters, R. D.; Helmy, A. A.; Kobashi, K. *Phys. Rev. B* **1983**, *28*, 2166−2171 and references therein; Stephens, P. W.; Birgeneau, R. J.; Majkraz, C. J.; Shirane, G. *Phys. Rev. B: Condens. Matter* **1983**, *28*, 452−454.

10.1021/ja9917215 CCC: $18.00
Published on Web 11/06/1999

possibly has a short-range antiferromagnetic order, and the γ phase which is orientationally disordered and paramagnetic just like liquid oxygen.

In spite of such an interest, the detailed characterization of the intermolecular potential in the oxygen dimer still continues to pose a challenge both to the experiments and to the theory of weak interactions. From an experimental point of view, it is very hard to measure properties giving direct insight into the interaction. As detailed later, the analysis of the available experimental findings often provides only limited information on the intermolecular potential. Additional efforts are needed to characterize the interaction in a wide range of intermolecular distances and as a function both of the relative molecular orientation and of the molecular-bond stretching. The main difficulties for the theory are inherent with the high dimensionality of a four-atom systems, and a further complexity is given by the open-shell nature of the monomer which is a $^3\Sigma_g^-$ in its ground electronic state.

Recently[8] we succeeded in measuring integral-scattering cross sections for the O_2-O_2 system with a control of the molecular alignment and with sufficient resolution to observe three quantum interference "glory" extrema. These data allow the first complete experimental characterization of the interaction in such a system, including an assessment of the role of the spin−spin interaction.

In the section of this paper titled Previous Studies we will review the previous experimental and theoretical works on the subject. In the following section we will present the experimental technique and results, while the representation of the potential-energy surface employed in this work will be described in the section by that name. A discussion of the analysis of the data and of the obtained potential-energy surfaces will follow in the last section.

Previous Studies

In the early 70s, Long and Ewing[9] were the first to reveal clearly the presence of O_2-O_2 dimers in the gas phase, by collision-induced spectroscopic studies at low temperature in the IR and visible range. From the analysis of the absorption spectrum they concluded that the dimer is stabilized both in the ground and the excited electronic state (dissociating to O_2 ($^1\Delta$) + O_2 ($^1\Delta$)) by a weak bond of van der Waals nature with well depths of 10.8 and 6.2 meV, respectively. The IR features were associated with end-over-end rotation of O_2-O_2, a floppy molecule with some of the dimers locked in a semirigid configuration and some others undergoing hindered rotations. Because of the low resolution of the spectroscopic data, the analysis gave no information on the spin−spin coupling effect and did not allow the determination of the structural properties for the complex: an equilibrium distance of $\sim 3.5 \pm 0.2$ Å was tentatively associated with a parallel (H) geometry.

The magnetic properties of oxygen dimers in the gas phase have also been studied: Reuss et al.[10] found O_4 molecules, formed in a supersonic molecular beam, to be paramagnetic from Stern-Gerlach deflection spectra of the dimers. On the contrary, more recently,[11] similar deflection spectra have lead to no appreciable paramagnetism and so to the conclusion that the ground state of the dimer is a singlet. Other studies considered dimers diluted in solid rare gas or nitrogen matrixes. Goodman and Brus[12] used a solid neon host matrix to isolate oxygen dimers: they measured high-resolution electronic spectra in the visible region and concluded that the dimer ground state is a singlet state (zero spin) and has a D_{2h} symmetry, with the two monomers lying parallel to each other in an H geometry.

Other sources of information on interactions in the dimer include also the second virial coefficient,[13] transport properties (shear viscosity and thermal conductivity,[14] and stimulated Raman self-broadening cross sections.[15] Although these studies have provided interesting additional insight on the system, they did not allow an accurate characterization of the interaction and in particular of the molecular anisotropy and of the role of spin.

There have also been extensive computational approaches. A first-order exchange perturbation calculation for the ground state potential energy surface of the dimer by van der Avoird and co-workers[16] was followed by other ab initio[17,18,19] and semi-empirical[20] calculations. Bussery and Wormer[21] have developed semi ab initio potential energy surfaces for $O_2(^3\Sigma_g^-)$ and $O_2(^1\Delta_g)$, and more recently Bussery et al.[22] have carried out full size-consistent ab initio calculations for the lowest singlet excited states of the dimer dissociating into $O_2(^1\Delta_g) + O_2(^1\Delta_g)$.

The remaining significant differences among all these calculations (for the singlet well depth, in the D_{2h} (H) configuration, values such as 3.0,[19] 19.1,[21] and 24.5[18] meV are reported) testify to the inadequacy of current quantum chemical methods to cope with this challenging problem.

A calculation of the magnetic coupling between oxygen molecules in the solid phase[23] has shown a strong anisotropy for the spin-coupling parameter, J (see eq 7 below), explaining the anomalously large libron splitting in $\alpha - O_2$. Furthermore, semi ab initio calculations[24] showed how the J parameter, related to the exchange interaction (i.e., to the overlap of outer electronic orbitals of two partners), contributes to stabilize the dimer in its singlet state in a D_{2h} structure.

To explain part of the "ozone deficit" problem, numerous experimental[25] and computational[18,26,27] studies have been carried out on the dynamics of the highly endothermic reaction

(8) Aquilanti, V.; Ascenzi, D.; Bartolomei, M.; Cappelletti, D.; Cavalli, S.; de Castro-Vitores, M.; Pirani, F. *Phys. Rev. Lett.* **1999**, *82*, 69−72.

(9) Long, C. A.; Ewing, G. E. *Chem. Phys. Lett.* **1971**, *9*, 225−229; *J. Chem. Phys.* **1973**, *58*, 4824−4834; Ewing, G. E. *Acc. Chem. Res.* **1975**, *8*, 185−192.

(10) van Deursen, A.; Reuss, J. *Int. J. Mass. Spectr. Ion Phys.* **1977**, *23*, 109−122.

(11) Malakhovskii, A.; Sominska, E.; Gedanken, A. *J. Chem. Soc., Faraday Trans.* **1996**, *92*, 1319−1322.

(12) Goodman, J.; Brus, L. E. *J. Chem. Phys.* **1977**, *67*, 4398−4407.

(13) Dymond, J. H.; Smith, E. B. *The virial coefficient of pure gases and mixtures: a critical compilation*; Clarandon Press: Oxford, 1980. *American Institute of Physics Handbook*, 3rd ed.; McGraw-Hill: New York, 1972.

(14) Laesecke, A.; Krauss, R.; Stephan, K.; Wagner, W. *J. Phys. Chem. Ref. Data* **1990**, *19*, 1089−1122.

(15) Millot, G.; Saint-Loup, R.; Santos, J.; Chaux, R.; Berger, H.; Bonamy, J. *J. Chem. Phys.* **1992**, *96*, 961−971.

(16) van Hemert, M. C.; Wormer, P. E. S.; van der Avoird, A. *Phys. Rev. Lett.* **1983**, *51*, 1167−1170; van der Avoird, A.; Wormer, P. E. S. *J. Chem. Phys.* **1984**, *81*, 1929−1939.

(17) Uhlik, F.; Slanina, Z.; Hinchliffe, A. *J. Mol. Struct.: THEOCHEM* **1993**, *285*, 273−276.

(18) Hernández, R.; Toumi, R.; Clary, D. C. *J. Chem. Phys.* **1995**, *102*, 9544−9556.

(19) Minaev, B. F.; Nikolaev, V. D.; Agren, H. *Spectrosc. Lett.* **1996**, *29*, 677−695.

(20) Varandas, A. J. C.; Pais, A. A. C. C. In *Theoretical and computational models for organic chemistry*; Formosinho, S. J., ed.; Kluwer: Dordrecht, 1991; pp 55−78.

(21) Bussery, B.; Wormer, P. E. S. *J. Chem. Phys.* **1993**, *99*, 1230−1239; Bussery, B. *Chem. Phys.* **1994**, *184*, 29−38.

(22) Bussery-Honvault, B.; Veyret, V. *J. Chem. Phys.* **1998**, *108*, 3243−3248.

(23) van der Avoird, A.; Brocks, G. *J. Chem. Phys.* **1987**, *87*, 5346−5360; Jansen, A. P. J.; van der Avoird, A. *J. Chem. Phys.* **1987**, *86*, 3583−3596; *J. Chem. Phys.* **1987**, *86*, 3597−3601.

(24) Bussery, B.; Umanskii, S. Ya.; Aubert-Frécon, M.; Bouty, O. *J. Chem. Phys.* **1994**, *101*, 416−423.

$$2O_2 \rightarrow O(^3P) + O_3(^1A_1) \quad (1)$$

(and its inverse) in the last few years. Those computations are sensitive to the repulsive part of the interaction because the reaction dynamics is assumed to involve highly vibrationally excited O_2 colliding at hyperthermal energies[25] and have been found to be inconsistent with observations.[26]

Experimental Technique and Results

We report in this paper molecular beam studies for the collisions between oxygen molecules. Such studies represent precious sources of information on interaction potentials especially when carried out with sufficiently high angular and energy resolution to allow the measurement of quantum interference effects. For molecule−molecule systems, these effects are often experimentally washed out when there is no control of rotational temperatures and of molecular orientations.

An early attempt[28] made with a hot effusive beam of fast rotating molecules emerging from a microwave discharge source allowed the measurement of total integral cross sections providing information on the interaction averaged over all mutual molecular orientations. In the last years considerable progress has been accomplished concerning production and characterization of beams emerging from supersonic sources,[29] permitting collisional studies with seeded beams of cold molecules, slowly rotating and with a controlled degree of the molecular alignment. Such an alignment could be probed for O_2 by measurements which exploit its paramagnetism.[30] Alignment effects also show up in scattering properties, especially in the glory phenomenon and on the overall size of cross sections,[31] providing an alternative quantitative probe for alignment also for nonparamagnetic species.[32] Recent progress on the understanding of the role of experimental conditions has been based on a detailed quantum mechanical analysis.[33,34]

This work is a continuation of experimental studies carried out in our laboratory on the O_2−Xe and O_2−Kr systems.[31,35] Measurements of the dependence of the total integral cross section on the rotational states and on the alignment degree of O_2 projectile molecules have been performed for the O_2−O_2 system in a wide velocity range, and some results have been recently anticipated.[8] The analysis of such data provides unique information both on the van der Waals component, including its dependence on the relative orientation of the molecules, and on the strength of the spin−spin coupling.

The Apparatus. The experimental apparatus employed for the measurements described in this paper is the same as that used recently for the O_2 rotational alignment study[29] and scattering experiments[31,35] with rare gases and, thus, will not be described here.

Two different beam sources have been used, operating under various regimes of pressure and temperature. Total (elastic + inelastic) integral cross sections are obtained through the measurement of the intensity loss of the velocity-selected beam as it crosses the scattering chamber, filled with the target gas (O_2, at the typical pressure range of 10^{-2}−10^{-3} torr) cooled down to liquid or solid air temperature, to decrease the quenching of the glory interference effect by the thermal motion of the target gas. For details on the angular and velocity resolutions see ref 35.

Scattering cross sections in the glory energy range have been measured under different experimental conditions, namely using both effusive (rotationally "hot") and supersonic seeded (ground vibro-rotational state) beams of oxygen, the latter involving a control of the alignment of the rotational angular momentum of the projectile molecule. As done previously, the absolute values of total cross sections have been obtained by an internal calibration based on direct measurements of the gas flowing in the scattering chamber and on the absolute value of He−Ar elastic scattering cross sections reported in ref 36.

Scattering Results: Experimental Informations from Rotationally "Hot" Beams. Effusive beams have been produced with a heated nozzle (source temperature, $T \sim 500$ K) of ∼1 mm in diameter with an O_2 pressure in the source of a few torr. The high rotational temperature of oxygen projectiles (several rotational states are populated, the most probable levels being $K = 9$−13) and the low translational temperature of the target O_2 molecules allow us to resolve the glory structure. Absolute total integral cross section results, plotted in Figure 1 as $Q(v)v^{2/5}$, as appropriate to emphasize quantum interference effects (the glory), clearly show three extrema. Error bars represent standard deviations over a large number of experimental runs. Curves are cross section calculations to be discussed below. These results extend previous ones,[28] covering a wider collisional velocity range under better experimental resolution.

In atom−atom collision systems, from the glory pattern it is possible to extract information on the potential well features,[37] while the absolute value of the cross section contains information about the long-range attraction.[38]

In the case of atoms colliding with molecules—even when vibrational effects can be neglected—the glory structure can be damped and shifted by the anisotropy of the interaction. These effects can be reduced by increasing the rotational temperature,[39] because when the molecular rotation period is short or comparable with the collision time, the cross-section feels an average of the intermolecular interaction. Moreover, the higher rotational levels are widely spaced in energy, and this limits the role of inelastic events.

(25) Slanger, T. G. *Science (Washington, D.C.)* **1994**, *265*, 1817−1818; Miller, R. L.; Suits, A. G.; Houston, P. L.; Toumi, R.; Mack, J. A.; Wodtke, A. M. *Science (Washington, D.C.)* **1994**, *265*, 1831−1837; Toumi, R.; Houston, P. L.; Wodtke, A. M. *J. Chem. Phys.* **1996**, *104*, 775−776.

(26) Mack, J. A.; Huang, Y.; Wodtke, A. M.; Schatz, G. C. *J. Chem. Phys.* **1996**, *105*, 7495−7503; Balakrishnan, N.; Billing, G. D. *Chem. Phys. Lett.* **1995**, *242*, 68−74; *J. Chem. Phys.* **1996**, *104*, 9482−9494; Szichman, H.; Varandas, A. J. C.; Baer, M. *J. Chem. Phys.* **1995**, *102*, 3474−3476; Varandas, A. J. C.; Wang, W. *Chem. Phys.* **1997**, *215*, 167−182.

(27) Lauvergnat, D.; Clary, D. C. *J. Chem. Phys.* **1998**, *108*, 3566−3573; Campos-Martínez, J.; Carmona-Novillo, E.; Echave, J.; Hernández, M. I.; Hernández-Lamoneda, R.; Palma, J. *Chem. Phys. Lett.* **1998**, *289*, 150−155.

(28) Brunetti, B.; Liuti, G.; Pirani, F.; Vecchiocattivi, F. *J. Chem. Phys.* **1981**, *74*, 6734−6741.

(29) Aquilanti, V.; Ascenzi, D.; Cappelletti, D.; Pirani, F. *Nature (London)* **1994**, *371*, 399−402.

(30) Aquilanti, V.; Ascenzi, D.; Cappelletti, D.; Pirani, F. *J. Phys. Chem.* **1995**, *99*, 13620−13626.

(31) Aquilanti, V.; Ascenzi, D.; Cappelletti, D.; Franceschini, S.; Pirani, F. *Phys. Rev. Lett.* **1995**, *74*, 2929−2932.

(32) Aquilanti, V.; Ascenzi, D.; Cappelletti, D.; Fedeli, R.; Pirani, F. *J. Phys. Chem. A* **1997**, *101*, 7648−7656.

(33) Aquilanti, V.; Ascenzi, D.; Cappelletti, D.; Pirani, F. *J. Phys. Chem. A* **1999**, *103*, 4424−4426.

(34) Aquilanti, V.; Ascenzi, D.; Cappelletti, D.; de Castro-Vitores, M.; Pirani, F. *J. Chem. Phys.* **1999**, *111*, 1−13.

(35) Aquilanti, V.; Ascenzi, D.; Cappelletti, D.; de Castro-Vitores, M.; Pirani, F. *J. Chem. Phys.* **1998**, *109*, 3898−3910.

(36) Nenner, T.; Tien, H.; Fenn, J. B. *J. Chem. Phys.* **1975**, *63*, 5439−5444; *J. Chem. Phys.* **1976**, *64*, 3902; Pirani, F.; Vecchiocattivi, F. *J. Chem. Phys.* **1977**, *66*, 372−373.

(37) Bernstein, R. B.; O'Brien, T. J. P. *Discuss. Faraday Soc.* **1965**, *40*, 35−44; *J. Chem. Phys.* **1967**, *46*, 1208−1209.

(38) Pirani, F.; Vecchiocattivi, F. *Mol. Phys.* **1982**, *45*, 1003−1013.

(39) Pirani, F.; Vecchiocattivi, F.; van den Biesen, J. J. H.; van den Meijdenberg, C. J. N. *J. Chem. Phys.* **1981**, *75*, 1042−1043.

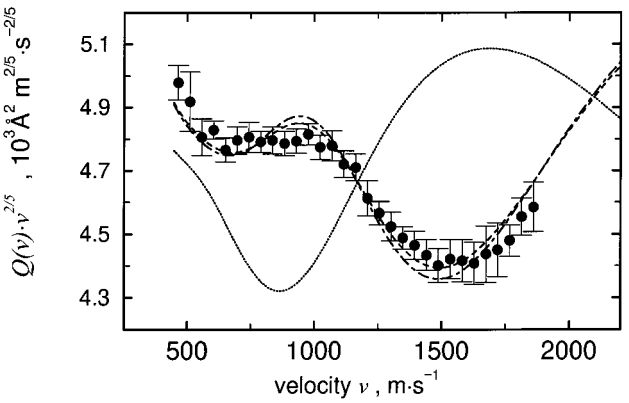

Figure 1. Total integral cross section $Q(v)$ for scattering of a rotationally hot O_2 effusive beam by O_2 target molecules. In this case anisotropy effects due to the relative mutual orientations can be neglected and only the spherical component of the PES has been used. The dotted-dashed curve is calculated excluding spin−spin interaction and the dashed curve is obtained considering the scattering on the three potential-energy curves of singlet, triplet, and quintet. Calculations performed with the semi ab initio PES of ref 21 are also reported as a dotted line.

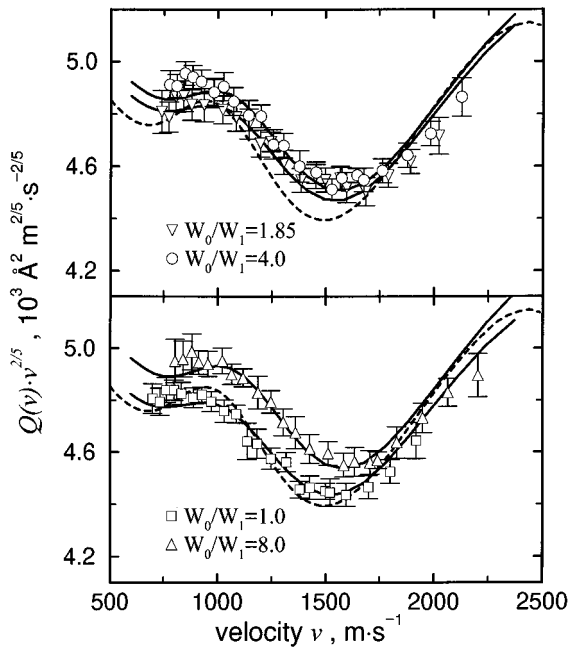

Figure 2. Total integral cross section $Q(v)$ for scattering of rotationally cold O_2 supersonic seeded beams by O_2 target molecules at four different degrees of molecular alignment W_0/W_1. Solid lines are quantum mechanical close-coupling calculations (see text). Dashed curve is as in Figure 1 and is repeated for comparison.

In the diatom−diatom case, anisotropy effects are expected to be larger. However, also, in this case, they can be partially removed by increasing the rotational temperature of one or both partners. Projectile oxygen molecules emerging from the hot effusive beam source exhibit a broad rotational distribution (about 20 rotational levels are significantly populated), and their average rotational period is $\sim 1 \times 10^{-12}$ s. The target O_2 molecules are kept in the cell at ~90 K, showing again a sufficiently ample rotational distribution with an average rotational period of $\sim 2 \times 10^{-12}$ s. The collision time ranges from $\sim 2 \times 10^{-12}$ s at the lowest experimental velocity to $\sim 5 \times 10^{-13}$ s at the highest one. Considering that O_2 molecules are homonuclear, so that the molecular configuration is repeated after a half period, and comparing collision times and rotational periods, at *low* and *intermediate* collision velocities (see Figure 1) the anisotropy of both diatomic partners is averaged toward the atom−atom limit, while at *high* velocities the projectile anisotropy is always averaged, and the target anisotropy can play some role only in the extreme velocity conditions, where the system approaches an atom−diatom limit. Therefore, scattering data with rotationally hot oxygen beams mainly probe the isotropic component of the interaction. In particular, the absolute value of the cross sections is sensitive to the long-range attraction, while the features of the glory pattern give information on the potential well.

Scattering Results: Experimental Information from "Cold" Beams with Alignment Control. Supersonic seeded beams are obtained expanding 2.5% O_2 mixtures in lighter gases at total stagnation pressures of ~1 atmosphere at room temperature through a nozzle of ~100-μm diameter. In the expansion the molecules experience several collisions with the carrier gas providing focusing along the beam axis, cooling to the lowest rotovibrational state ($K = 1$), and alignment of rotational angular momentum. Since these molecules rotate slowly (average period of $\sim 8 \times 10^{-12}$ s), the study of their collisions is a probe of the interaction anisotropy in the whole velocity range presented in this work. The alignment degree, given by the ratio W_0/W_1 of the weights for the two helicity states possible for $K = 1$ (M equal to either 0 or 1) can be measured and controlled as detailed in refs 29, 31, 35.

Absolute total integral scattering cross sections are reported in Figure 2 as a function of the collision velocity v for four values of the alignment degree W_0/W_1 of the O_2 projectile molecules. The figure shows that, increasing W_0/W_1, scattering cross sections present an overall average increase and a shift in the velocities corresponding to the glory extrema. In the figure the dashed line is the same as in Figure 1 and allows comparison with data obtained with rotationally hot effusive beams. Other curves in the figure are calculations (see below). These results obtained with rotationally cold and aligned O_2 molecules will serve to extract information on anisotropy of interactions at long range and in the well region.

Other Experimental Results. Other experimental measurements on the O_2-O_2 system are available in the literature as detailed in the previous sections.

In addition to the scattering cross sections, in the following analysis we will also consider the second virial coefficient $B(T)$, plotted in Figure 3 and reported in Table 1 for the temperature range for which it is available.[13] The second virial coefficient at high temperatures mainly depends on the spherical component of the interactions, while at low temperatures it is also influenced by their anisotropy.

Representation of the Potential Energy Surfaces

The geometry of the O_2-O_2 dimer and its interaction energy will be described in Jacobi coordinates appropriate for four-body systems and shown in Figure 4. The vector pointing from the center of mass of molecule a to the center of mass of molecule b is denoted **R** and has modulus R. The diatomic internuclear vectors are denoted as $\mathbf{r}_a$ and $\mathbf{r}_b$; they define the orientation of the two oxygen molecules with bond lengths r_a and r_b. In a body fixed reference frame chosen with the z axis to coincide with the direction of **R**, the set of internal coordinates, on which the interaction energy depends, is given by the intermolecular distance R, the bound distances r_a and r_b, and the angles θ_a, θ_b and $\phi = \phi_a - \phi_b$.

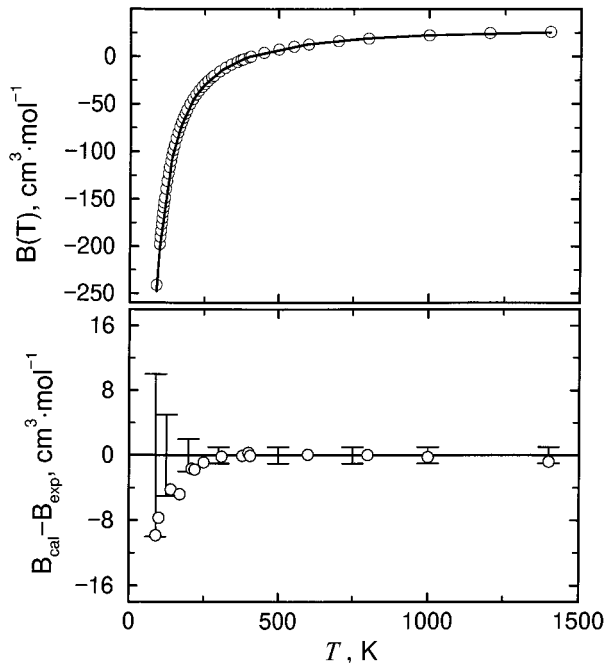

Figure 3. In the upper panel is reported the experimental second virial coefficient $B(T)$ for the O_2-O_2 system and it is compared with calculations performed using the present potential-energy surfaces. (Calculations with or without spin−spin contribution are not distinguishable in the scale of the figure.) In the lower panel is plotted the deviation of the calculated second virial coefficient B_{cal} including spin−spin contribution (see Table 1) from the experimental results B_{exp}. The experimental uncertainties are also shown at some indicative temperatures.

Table 1. Experimental and Calculated Second Virial Coefficient $B(T)$ as a Function of Temperature[a]

	this work			
T (K)	full PES	full PES without spin	V^{000}	experimental ref 13
90	−251	−248	−208	−241 ± 10
100	−205	−202	−171	−197 ± 7
140	−108	−107	−91	−104 ± 5
170	−74	−73	−61	−69 ± 4
210	−47	−46	−37	−45 ± 2
220	−42	−41	−33	−40 ± 2
250	−30	−29	−22	−29 ± 2
310	−14	−14	−8.1	−14 ± 1
380	−3.0	−2.8	2.0	−3 ± 1
400	−0.7	−0.4	4.1	−1 ± 1
406	0.0	0.2	4.7	0 ± 1
600	13	13	17	13 ± 1
800	19	19	22	19 ± 1
1000	22	22	25	22 ± 1
1400	25	25	27	26 ± 1

[a] The calculations have been performed using the present potential-energy surface (full PES), excluding the spin−spin interaction, and using only the spherical component $V^{000}(R)$.

In this work, we will consider r_a and r_b as fixed and, thus, the molecules as rigid rotors. The interaction can be expanded in spherical harmonics, separating the radial and the angular dependencies[16,21]

$$V(R,\theta_a\theta_b,\phi) = 4\pi \sum_{L_a,L_b,L} V^{L_aL_bL}(R) Y^{L\,0}_{L_aL_b}(\theta_a,\theta_b,\phi) \qquad (2)$$

with L_a, $L_b = 0, 1, 2, \ldots$ and $|L_a - L_b| \le L \le L_a + L_b$. The angular functions $Y^{L0}_{L_aL_b}$ are bipolar spherical harmonics

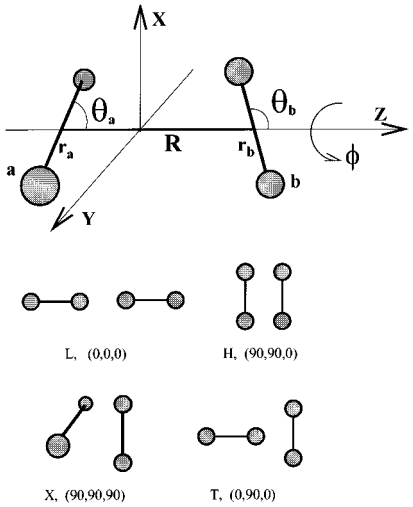

Figure 4. Orientation angles θ_a, θ_b, and ϕ and selected relevant geometries for the oxygen dimer system.

$$Y^{L\,0}_{L_aL_b}(\theta_a,\theta_b,\phi) = (2L+1)^{1/2}\sum_m (-)^{L_a-L_b}\begin{pmatrix} L_a & L_b & L \\ m & -m & 0 \end{pmatrix} Y_{L_am}(\theta_a,\phi_a) Y_{L_b-m}(\theta_b,\phi_b) \qquad (3)$$

where Y_{L_am} and Y_{L_b-m} are spherical harmonics, (:::) is a Wigner $3-j$ symbol, and $-\min(L_a,L_b) \le m \le \min(L_a, L_b)$.

The radial coefficients $V^{L_aL_bL}(R)$ include different types of contributions to the interaction potential (electrostatic, dispersion, repulsion due to overlap, induction, spin-spin coupling, ...).

In previous applications (such as to N_2-N_2[40] and to O_2-O_2,[21] in order to represent results of calculation on grids of intermolecular distances and geometries, the spherical harmonic expansion included a large number of terms (for the oxygen dimer more than 20[21]) each one defined by functions which at least contain two variable parameters. Seeking for a more compact representation of the interaction, we propose a harmonic expansion consisting of four terms: this is the minimum number of moments needed to characterize four basic configurations of the dimer (to be referred to in Figure 4). Contributions to the interaction of higher order are less and less important and will not be explicitly included, therefore the terms retained in our representation must be considered as "effective" because they are adjusted to account for possible higher order contributions. Thus the present treatment extends the usual approach to the atom−diatom case, for which the interaction is developed in a polynomial Legendre expansion truncated to an effective anisotropic second-order term. One important advantage in using such a simplified representation is that the terms in the expansion lead to a small number of parameters, to be varied in the procedure of fitting to the experimental data.

Since O_2 is a homonuclear molecule, only even moments contribute to the sum in eq 2:

$$V(R,\theta_a,\theta_b,\phi) = 4\pi\{V^{000}(R) + V^{202}(R)[Y^{20}_{20}(\theta_a,\theta_b,\phi) + Y^{20}_{02}(\theta_a,\theta_b,\phi)] + V^{220}(R) Y^{00}_{22}(\theta_a,\theta_b,\phi) + V^{222}(R) Y^{20}_{22}(\theta_a,\theta_b,\phi) + \ldots\} \qquad (4)$$

The first term of the expansion, V^{000}, represents the isotropic component of the interaction, while V^{202}, V^{220}, and V^{222} describe

(40) van der Avoird, A.; Wormer, P. E. S.; Jansen, A. P. J. *J. Chem. Phys.* **1986**, *84*, 1629−1635.

the overall anisotropy. Higher order terms will be neglected, and the truncated expansion will be found appropriate to analyze the present experimental data and the second virial coefficient.

Also, by inserting proper values of the three angles θ_a, θ_b, and ϕ in the explicit expressions of bipolar spherical harmonics, the interaction potentials of the four basic configurations H, X, T, L (Figure 4) are given by

$$V^{H}(R) = V^{000}(R) - \sqrt{5}V^{202}(R) + \sqrt{5}V^{220}(R) + \frac{5}{\sqrt{14}}V^{222}(R)$$

$$V^{X}(R) = V^{000}(R) - \sqrt{5}V^{202}(R) - \frac{\sqrt{5}}{2}V^{220}(R) - 2\frac{5}{\sqrt{14}}V^{222}(R)$$

$$V^{T}(R) = V^{000}(R) + \frac{\sqrt{5}}{2}V^{202}(R) - \frac{\sqrt{5}}{2}V^{220}(R) + \frac{5}{\sqrt{14}}V^{222}(R)$$

$$V^{L}(R) = V^{000}(R) + 2\sqrt{5}V^{202}(R) + \sqrt{5}V^{220}(R) - 2\frac{5}{\sqrt{14}}V^{222}(R) \quad (5)$$

These expressions can be inverted, to give

$$V^{000}(R) = \frac{1}{9}[2V^{H}(R) + 2V^{X}(R) + 4V^{T}(R) + V^{L}(R)]$$

$$V^{202}(R) = \frac{2}{9\sqrt{5}}[-V^{H}(R) - V^{X}(R) + V^{T}(R) + V^{L}(R)]$$

$$V^{220}(R) = \frac{1}{9\sqrt{5}}[4V^{H}(R) - 2V^{X}(R) - 4V^{T}(R) + 2V^{L}(R)]$$

$$V^{222}(R) = \frac{\sqrt{14}}{45}[V^{H}(R) - 2V^{X}(R) + 2V^{T}(R) - V^{L}(R)] \quad (6)$$

Once the interactions for the four limiting geometries V^{H}, V^{X}, V^{T}, and V^{L} are obtained, the effective radial coefficients $V^{000}(R)$, $V^{202}(R)$, $V^{220}(R)$, $V^{222}(R)$ allow the representation of the potential energy surface through eq 4. The parameterization of the radial coefficients is reported in Appendix A.

When the spin−spin interaction is introduced, three distinct potential energy surfaces arise, corresponding to the singlet (total spin $S = 0$), triplet ($S = 1$), and quintet ($S = 2$) states of the dimers, obtained from the coupling of the two spins ($S_a = S_b = 1$) of the monomers in their ground $^3\Sigma$ state. Splittings between these surfaces are caused by an exchange interaction, due to the overlap of outer-shell electronic clouds and which can be represented in the form of a Heisenberg spin Hamiltonian $-2J\mathbf{S_a}\cdot\mathbf{S_b}$,[16] where $\mathbf{S_a}$ and $\mathbf{S_b}$ are the monomer electron spin operators and J is the coupling parameter which is linked to the exchange integral and depends both on the distance between the O_2 molecules and on their orientations, just as the van der Waals component of the interactions.

Eigenvalues for the Heisenberg Hamiltonian are $4J$ for $S = 0$, $2J$ for $S = 1$, and $-2J$ for $S = 2$, so that the interaction for each of the multiplet states can be described as:

$$V^{(S=0)} = V + 4J$$

$$V^{(S=1)} = V + 2J$$

$$V^{(S=2)} = V - 2J \quad (7)$$

A convenient representation of the radial and angular dependencies of the spin interaction follows along the lines of eq 4 and is given in terms of a spherical harmonic expansion consisting of the first four terms $J^{000}(R)$, $J^{202}(R)$, $J^{220}(R)$, and $J^{222}(R)$

$$J(R,\theta_a,\theta_b,\phi) = 4\pi\{J^{000}(R) + J^{202}(R)[Y^{20}_{20}(\theta_a,\theta_b,\phi) + Y^{20}_{02}(\theta_a,\theta_b,\phi)] + J^{220}(R)Y^{00}_{22}(\theta_a,\theta_b,\phi) + J^{222}(R)Y^{20}_{22}(\theta_a,\theta_b,\phi)\} \quad (8)$$

where the radial coefficients $J^{ijk}(R)$ are parametrized as follows

$$J^{ijk}(R) = a^{ijk}\exp(-b^{ijk}R)$$

The harmonic expansion (8) allows reproduction of the general features of the complete spherical harmonic expansion of ref 16 in particular, the orientational dependence of the coupling term J yields positive values for crossed geometry (X) but gives antiferromagnetic coupling ($J < 0$) for parallel (H), T-shape (T), and linear (L) configurations. The functional form of each $V^{(S)}$ state can be now given[16,21] by separately expanding V and J according to eqs 4 and 8 and subsequently combining them.

The PES: Analysis and Discussion

The van der Waals Interaction. The reliability of the representation of a diatom−diatom potential energy surface with four effective terms has been firstly tested on a recent accurate semi-empirical potential for the N_2 dimer from this laboratory.[41] Reproduction of detailed features required only slight modifications of the original first four terms of the expansion, confirming the validity of the approach and its perspective applications to other systems.

The data from rotationally hot effusive beam scattering has been analyzed using the average interaction only, i.e., using the first term of the spherical harmonic expansion, V^{000}; the cross section calculations have been performed following a JWKB method. To assess the sensitivity of our experimental data and the quality of the obtainable information on the interaction, we tested the more accurate PES[21] available in the literature. In Figure 1 we have reported calculated cross sections (as dotted lines) by using the V^{000} term of the semi ab initio PES:[21] the glory pattern is dephased with respect to the experimental one and has a different frequency. This marked difference suggests that the negative area of the V^{000} potential needs to be much larger than that calculated in ref 21, and this is also in the same direction as indicated by comparison with the data on the second virial coefficient.[21]

In this work the V^{000} term of the PES has been parametrized as a Morse-spline-van der Waals (MSV) potential (see Appendix A): the C^{000} (long range dispersion coefficient) value has been obtained by fitting the absolute value of the rotationally hot scattering cross sections, the ϵ (well depth) and R_m (well location) parameters have been varied until the best fit for position and frequency of the glory oscillations is obtained. Calculations for scattering cross sections - from the best fit V^{000} term - are also shown in Figure 1 as dot-dashed lines.

The potential parameters so obtained (See Table 2) were found to be in good agreement with those estimated by correlation formulas based on the average polarizability of the

(41) Cappelletti, D.; Vecchiocattivi, F.; Pirani, F.; Heck, E. L.; Dickinson, A. S. *Mol. Phys.* **1998**, *93*, 485−499.

Table 2. Parameters of the Potential-Energy Surface (see Appendix A) for the O_2-O_2 System As Determined in the Present Work[a]

V^{000}	
ϵ (meV)[b]	11.7 (±0.6)
R_m (Å)	3.90 (±0.08)
β	6.7
C^{000} (meV Å^6)	5.3 (±0.5) × 10^4
x_1	1.12
x_2	1.55
V^{202}	
A^{202} (meV)	7.7 (±1.5) × 10^6
c^{202} (Å^{-1})	4.0 (2%)
d^{202} (Å^{-2})	−0.060 (2%)
C^{202} (meV Å^6)	6.12 × 10^3
V^{220}	
A^{220} (meV)	5.0 (±1.5) × 10^6
c^{220} (Å^{-1})	3.83 (2%)
V^{222}	
A^{222} (meV)	−4.0 (±1.5) × 10^6
c^{222} (Å^{-1})	3.83 (2%)

[a] Estimated uncertainties are in parentheses. [b] 1 meV = 9.648 × 10^{-2} kJ·mol^{-1}.

oxygen molecule.[42] This represents a further proof of the fact that integral cross sections measured with rotationally hot beams mainly probe the spherical part of the interaction. Nonetheless, we notice (in Figure 1) that the exclusive use of the spherical term V^{000} in the O_2-O_2 case fails to fully reproduce the amplitude of glory oscillations in the low-velocity range (differently from what had been observed in the N_2-N_2 case:[41] experimental cross sections appear to present a partial quenching with respect to those from calculations, implying the presence of a residual anisotropy, to be attributed (see below) to the spin−spin interaction.

The analysis of scattering cross sections measured with rotationally cold beams of aligned oxygen molecules has been based on a quantum close-coupling calculation of the scattering matrix, performed using the MOLSCAT package[43] and following the lines of calculations adopted for $Kr-O_2$ and $Xe-O_2$ systems (see refs 31 and 35).

As previously observed, oxygen molecules in the scattering chamber have a sufficiently high rotational temperature (∼90 K, average rotational period ∼2.0 × 10^{-12} s) to basically behave as pseudo atoms during the collision with an oxygen molecule aligned in the ground rotational state $K = 1$ (average rotational period ∼8.0 × 10^{-12} s). On this basis, the MOLSCAT program has been adapted to calculate the cross section for an aligned oxygen molecule with a pseudoatom of mass equal to 32 amu (see Appendix B for the reduction of the potential-energy surface to the atom−diatom limit), allowing the characterization of the main anisotropic term $V^{202}(R)$. In particular, the increase of the value of the cross section with the degree of alignment of the molecules has been used to probe the long-range part of the anisotropy, while the shift of the glory position allowed the determination of the anisotropy in the well region. The check of the amplitude of the quantum oscillations has been performed as discussed below including the effect of the spin−spin coupling.[44] The results are reported in Figure 2 as continuous lines.

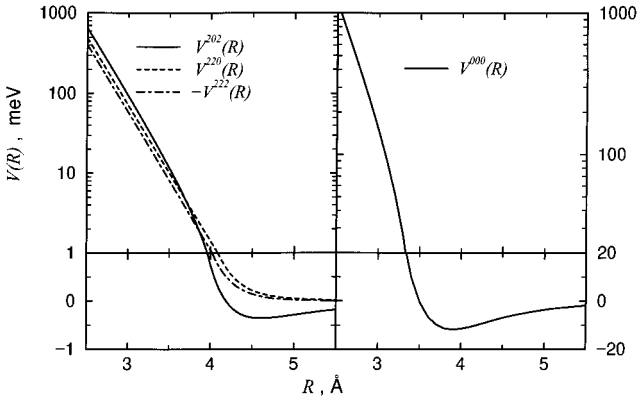

Figure 5. Radial coefficients $V^{ijk}(R)$ as a function of the intermolecular distance R as obtained in the present work.

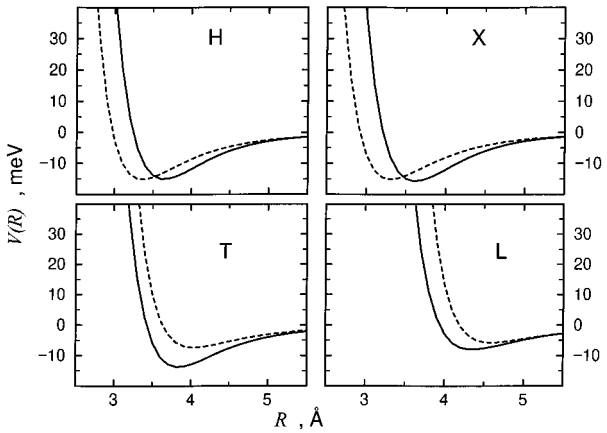

Figure 6. Cuts of the potential-energy surfaces excluding spin−spin interaction, for relevant geometries of the O_2 dimer (see Figure 4) as obtained by the present analysis (continuous lines) and by the previous semi ab initio PES.[21]

The final refinment of the anisotropy has been done including the remaining two minor (but not negligible) anisotropic terms, V^{220} and V^{222}.[45] The full anisotropic PES has been checked on second virial coefficient $B(T)$ in the full temperature range and scattering cross sections. $B(T)$ values have been calculated using a method based on the expressions for two linear molecules presented by Pack,[46] including the first quantum corrections due to the relative translational and rotational motions, with the Coriolis term in the latter. The same approach had been used previously for the N_2-N_2 system.[40,41] The calculated values of $B(T)$ are in good agreement with experimental ones, as shown in Figure 3 and Table 1.

The best-fit radial functions $V^{ijk}(R)$ are plotted in Figure 5, while cuts of the PES for the four limiting geometries are reported in Figure 6 together with the corresponding values of Bussery et al.,[21] for a comparison.

The best-fit potential parameters are reported in Table 2 together with the estimated uncertainties. A comment on the relative extent of anisotropic terms is here in order: The main contribution to anisotropy derives from the first $V^{202}(R)$ which

(42) Cambi, R.; Cappelletti, D.; Liuti, G.; Pirani, F. *J. Chem. Phys.* **1991**, *95*, 1852−1861.

(43) Hutson, J. M.; Green, S. MOLSCAT computer code, distributed by Collaborative Computational Project No. 6 of the Engineering and Physical Sciences Research Council (UK). http://www.gis.nasa.gov/molscat/. (accessed May 1999).

(44) Integral cross section calculations for the full dimensional problem, i.e., considering the scattering between two linear rigid rotors, are still prohibitively expensive and time-consuming.

(45) In the analysis we have neglected electrostatic quadrupole−quadrupole contributions to the interaction because of the very small quadrupole moment of the oxygen molecule (see Stogryn, D. E.; Stogryn, A. P. *Mol. Phys.* **1966**, *4*, 371−393).

(46) Pack, R. T. *J. Chem. Phys.* **1983**, *78*, 7217−7222.

Table 3. Parameters for the Coupling Term J which describes Spin−Spin Interaction in the $(O_2)_2$ Dimer System

	J^{000}	J^{202}	J^{220}	J^{222}
a^{ijk} (meV)[a]	-1.7×10^6 (40%)	-1.3×10^6 (40%)	-1.7×10^6 (40%)	2.1×10^6 (40%)
b^{ijk} (Å^{-1})	3.96	4.09	4.30	4.63

[a] Estimated uncertainties are in parentheses.

accounts for ~30% of the global interaction, while $V^{220}(R)$ and $V^{222}(R)$ are much smaller (<5%), but they are necessary to introduce the proper angular dependence and thus give a realistic description of the PES.

Role of the Spin−Spin Interaction. As already anticipated, scattering results performed with effusive beams containing rotationally "hot" oxygen molecules show a quenching in the glory amplitudes at low collision velocities which we attribute to the role of the spin−spin interaction and, specifically, to its spherical component $J^{000}(R)$, i.e., independent of averaging over molecular orientations. This small but appreciable quenching allows an estimate of the magnitude of the $J^{000}(R)$ term, which is expected to be only a small fraction of the whole interaction. As a consequence, the relatively small anisotropy introduced by the $J^{000}(R)$ term influences only the glory amplitude (and not the frequency and location of the extrema) and the $B(T)$ values at low temperature.

To take into account the spin−spin interaction in the analysis of integral-scattering cross sections and second virial coefficients it must be noted that, as a consequence of the conservation of total spin quantum number S of the system during a collision, transitions between surfaces with different spin values are not allowed, and the presently measured total integral cross sections $Q(v)$ are the weighted sum of the three partial cross sections $Q^{S=0}(v)$, $Q^{S=1}(v)$, and $Q^{S=2}(v)$, which, respectively, refer to singlet, triplet, and quintet surfaces

$$Q(v) = \frac{Q^{S=0}(v) + 3Q^{S=1}(v) + 5Q^{S=2}(v)}{9} \qquad (9)$$

where the weighting factors are determined by degeneracies associated with each spin state. An analogous expression applies when similarly extending the treatment of the second virial coefficient $B(T)$.

A calculation using the present best fit $V^{000}(R)$ and the ab-initio $J^{000}(R)$,[16] obtained by properly compacting J to four terms as in the section titled "Representation of the Potential Energy Surfaces", has been compared with the data measured with rotationally hot beams (not reported in Figure 1) but doesn't show any appreciable quenching in the glory amplitude. This indicates the need of a larger spin−spin contribution.

Therefore, the pre-exponential coefficient a^{000} of the radial term $J^{000}(R)$ has been increased until an appreciable quenching appears in the calculations. Results presented in Figure 1 as a dashed line have been obtained by using a scaling factor of 2.5 (with respect to the ab initio results), which we consider consistent with the experimental data. The same factor has been used for scaling the three remaining coefficients a^{ijk} of the radial terms J^{ijk} in order to obtain the full PESs and to calculate cross sections for aligned molecules and second virial coefficient at low T (see Figures 2 and 3). The best fit parameters for the spin−spin interaction are reported in Table 3. The present study also allows the determination of an upper limit for J, forcing the quenching of the calculated cross sections to the limit of experimental error bars of the data in Figure 1 (not reported), with a further increase of the pre-exponential a^{ijk} coefficients. This determination relies on the assumption that the quenching of the glory structure in effusive data is exclusively due to spin-dependent interaction. This upper limit for J corresponds to a 40% increase of the a^{ijk} best-fit coefficients reported in Table 3.

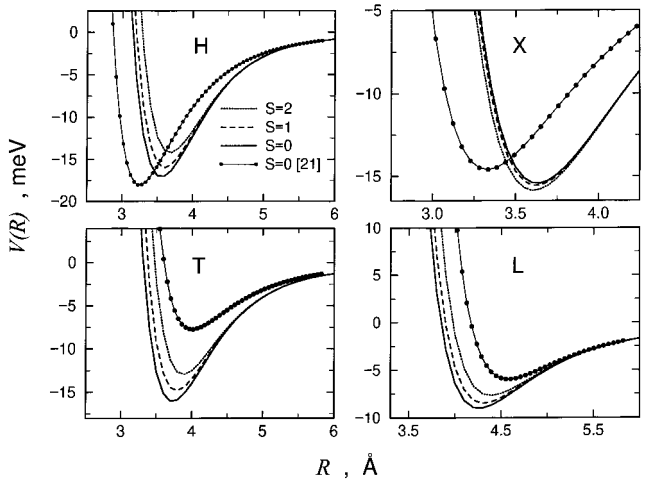

Figure 7. Cuts of the potential-energy surfaces for relevant geometries of the O_2 dimer (see Figure 4) and including spin−spin interaction ($S = 0$ singlet, $S = 1$ triplet, and $S = 2$ quintet states) as obtained by the present analysis. Also shown are semi ab initio results for the singlet state.[21]

Table 4. Equilibrium Distances R_m and Binding Energies E for Singlet, Triplet, Quintet, and Spin-Averaged Potential Surfaces in Selected Geometries for the Oxygen Dimer System

	$V^{(S=0)}$		$V^{(S=1)}$		$V^{(S=2)}$		V		N_2-N_2[a]	
	E^b	$R_m{}^c$	E^b	$R_m{}^c$	E^b	$R_m{}^c$	E_b	$R_m{}^c$	E^b	$R_m{}^c$
H	17.0	3.56	15.9	3.61	14.3	3.68	15.1	3.64	10.9	3.68
X	15.3	3.63	15.5	3.62	16.0	3.60	15.8	3.61	11.5	3.67
T	16.0	3.74	14.7	3.79	12.9	3.88	13.7	3.84	12.0	4.10
L	9.1	4.26	8.6	4.30	7.7	4.38	8.10	4.34	3.4	4.81
V^{000}	13.3	3.81	12.4	3.86	11.1	3.94	11.7	3.90	9.5	4.10

[a] Corresponding results for the N_2 dimer are shown for comparison in the last two columns. These numerical values correspond to data shown graphically in Figure 12 of ref 41. [b] meV. Absolute uncertainties are estimated as ±0.8 meV. 1 meV = 9.648×10^{-2} kJ·mol^{-1}. [c] Å. Absolute uncertainties are estimated as ±0.07 Å.

Concluding Remarks. Potential-energy curves for singlet, triplet, and quintet states in selected geometries are plotted in Figure 7, where results for the lowest singlet state are compared with ab initio calculations of ref 21.

It can be noted that, in agreement with ab initio calculations, the planar rectangular H geometry is the most favorable for the singlet state: this is therefore the configuration of the ground state for the dimer. It is also favored with respect to other geometries in the triplet state while the X structure results in being the most stable for the quintet state. Such a stabilization of the X geometry for the quintet state originates, as also pointed out in ref 21, from the different sign of the spin-coupling parameter J which is positive (i.e., ferromagnetic) for the previous configuration and negative (i.e., antiferromagnetic) for the latter. Table 4 reports the main features (equilibrium distances R_m and binding energies E) for singlet, triplet, and quintet potential-energy surfaces for the four basic geometries. Data for the average over spin states, which represent the pure van der Waals interactions, are also shown together with the corresponding results for the N_2-N_2 system of ref 41. Absolute

uncertainties are estimated as ±0.8 meV for E and ±0.07 Å for R_m. Relative values are accurate to the digits given.

It is interesting to note that, differently from what is observed in O_2-O_2, the most stable geometry for N_2-N_2 has a T shape. This can be attributed to the non-negligible role of quadrupole−quadrupole interaction for the nitrogen case.[41]

Indeed, the nature of these interactions can be shown to be mainly due to pure van der Waals forces, the spin−spin interaction being only of the order of ∼15%—perhaps less than would have been anticipated by Pauling,[2] but larger than that maintained by others.[16]

Present results confirm previous experimental evidence concerning the planar rectangular H geometry of dimers of oxygen molecules in the solid α phase (stable for temperatures between 0 and 23.9 K) and in the β phase (stable in the temperature range $23.9 < T < 43.8$ K), both such phases having an antiferromagnetic character.[7] The spectroscopic work of ref 12 also indicated an H geometry for the singlet ground state of the dimers diluted in a solid neon host matrix. For the higher lying triplet and quintet states, D_{2h} (H geometry) or D_{2d} (X geometry) symmetries have been found.

Our estimate of the spin−spin coupling term in the distance range corresponding to that for the equilibrium of the dimer can be an ingredient for modeling magnetic properties in solid O_2.

The characterization of the three surfaces will contribute to the assignment of features of absorption spectra and of spectral broadening due to dimer formation. Moreover, since the bond length and, thus, the polarizability of O_2 molecules do not appreciably change for electronic excited states $^1\Delta$ and $^1\Sigma$ (see also ref 22), the corresponding excited surfaces of the dimer are expected to behave similarly to the van der Waals component in the ground electronic state, while spin−spin coupling are absent there. All these surfaces are relevant for the elementary processes of ozone chemistry.

Acknowledgment. We thank Beatrice Bussery-Honvault (Rennes) and Alan Dickinson (Newcastle) for contributions to this work, which is supported by the Ministero dell'Università e della Ricerca Scientifica e Tecnologica (MURST) and by the Ente per le Nuove Tecnologie, l'Energia e l'Ambiente (ENEA).

Appendix A - Parametrization of the Radial Terms

The effective radial coefficients in eqs 4 and 7 have been represented by standard parametrizations. The isotropic $V^{000}(R)$ component has been described by the following MSV (Morse−spline−van der Waals) parametrization, scaled for location R_m and depth ϵ of the potential well

$$x = \frac{R}{R_m}, \quad f(x) = \frac{V_0(R)}{\epsilon} \tag{10}$$

Morse for $x \le x_1$

$$f(x) = \exp[-2\beta(x-1)] - 2\exp[-\beta(x-1)] \tag{11}$$

spline for $x_1 < x < x_2$

$$f(x) = b_1 + (x-x_1)\{b_2 + (x-x_2)[b_3 + (x-x_1)b_4]\} \tag{12}$$

van der Waals for $x \ge x_2$

$$f(x) = -\left(\frac{C^{000}}{\epsilon R_m^6}\right)x^{-6} \tag{13}$$

The β parameter, which defines the shape of the potential well, is fixed at 6.7, as is characteristic of van der Waals forces;[47] x_1 and x_2 are chosen, as for other previous cases,[31,35] in the neighborhood of 1.1 and 1.5; then b_1, b_2, b_3, and b_4—the spline parameters—are automatically fixed by imposing the rule that functions join with the same value and the same derivative at x_1 and x_2. The free parameters (related to the isotropic component of the interaction) in the fit are ϵ, R_m, and C^{000}.

The $V^{202}(R)$ term, which describes the anisotropy of short-range repulsive interaction and long-range dispersion forces, has been parametrized as

$$V^{202}(R) = A^{202}\exp(-c^{202}R - d^{202}R^2) - \frac{C^{202}}{R^6} \tag{14}$$

where the exponential function describes the behavior of short-range repulsion, and the C^{202} coefficient quantifies the long-range anisotropy. According to the Buckingham notation[48] in the case of pure dipole−dipole attraction

$$\frac{C^{202}}{C^{000}} \approx \frac{1}{\sqrt{5}}\frac{\alpha_{\parallel} - \alpha_{\perp}}{\alpha_{\parallel} + 2\alpha_{\perp}} \approx 0.116 \tag{15}$$

where $\alpha_{\parallel}$ and $\alpha_{\perp}$ are the collinear and perpendicular polarizabilities of the diatomic molecule,[35] respectively.

The $V^{220}(R)$ and $V^{222}(R)$ terms have been represented as:

$$V^{220}(R) = A^{220}\exp(-c^{220}R) \tag{16}$$

$$V^{222}(R) = A^{222}\exp(-c^{222}R) \tag{17}$$

In the present work c^{222} has been taken to be equal to c^{220}. Thus, the free parameters (related to the anisotropic component of the interaction) in the fit are A^{202}, c^{202}, d^{202}, A^{220}, A^{222}, and $c^{220} = c^{222}$. The best-fit parameters with relative uncertainties are reported in Table 2.

Appendix B - The Atom−Diatom Limit

For the analysis of integral scattering cross section measured in our laboratory a reduction of the dimensionality of the problem arises when the interaction can be averaged over the orientation of one of the molecules. In this pseudo atom−diatom representation (see also ref 41)

$$V(R,\theta) = V^{000}(R) + \sqrt{5}V^{202}(R)P_2(\cos\theta) + 3V^{404}(R)P_4(\cos\theta) + \sqrt{13}V^{606}(R)P_6(\cos\theta) + \ldots \tag{18}$$

where the $V^{L_aL_bL}(R)$ are moments of the spherical harmonic expansion and $P_\lambda(\cos\theta)$ are Legendre polynomials.

Allowing for oinly the first two terms of this expansion and introducing the spin coupling

$$V^{(S=0)}(R,\theta) = V^{000}(R) + \sqrt{5}V^{202}(R)P_2(\cos\theta) + 4[J^{000}(R) + \sqrt{5}J^{202}(R)P_2(\cos\theta)] \tag{19}$$

$$V^{(S=1)}(R,\theta) = V^{000}(R) + \sqrt{5}V^{202}(R)P_2(\cos\theta) + 2[J^{000}(R) + \sqrt{5}J^{202}(R)P_2(\cos\theta)] \tag{20}$$

$$V^{(S=2)}(R,\theta) = V^{000}(R) + \sqrt{5}V^{202}(R)P_2(\cos\theta) - 2[J^{000}(R) + \sqrt{5}J^{202}(R)P_2(\cos\theta)] \tag{21}$$

JA9917215

(47) Aquilanti, V.; Cappelletti, D.; Pirani, F. *Chem. Phys.* **1996**, *209*, 299−311.
(48) Buckingham, A. D. *Adv. Chem. Phys.* **1967**, *12*, 107−142.